J Mater Sci: Mater Electron (2021) 32:8603–8614

Optimization mechanism of Li_2ZrO_3-modified lithium-rich cathode material $Li[Li_{0.2}Ni_{0.2}Mn_{0.6}]O_2$ for lithium-ion batteries

Taolin Zhao[1,2], Jiangang Shen[1], Rixin Ji[1], Yueting Zhang[1], and Yuhua Wang[1,2,*]

[1] School of Materials Science and Engineering, Shijiazhuang Tiedao University, 050043 Shijiazhuang, China
[2] Hebei Key Laboratory of Advanced Materials for Transportation Engineering and Environment, 050043 Shijiazhuang, China

Received: 25 October 2020
Accepted: 7 February 2021
Published online: 18 March 2021

ABSTRACT

To achieve lithium-ion batteries with high energy and power density, it is necessary to develop alternative high-capacity cathode materials for traditional $LiCoO_2$ or $LiFePO_4$, such as lithium-rich manganese-based cathode materials. However, there are still some practical problems that Li-rich materials need to be further improved, such as structure transformation issue and poor rate capability. Here, the modification of $Li[Li_{0.2}Ni_{0.2}Mn_{0.6}]O_2$ cathode material by lithium-ion conductor (Li_2ZrO_3) has been achieved by a sol–gel method, and the optimization mechanism is preliminarily explored. The first charge/discharge specific capacities of the modified material coated with 1 wt.% Li_2ZrO_3 can reach 272.1 and 196.1 mAh g^{-1} at 0.5 C, which are obviously higher than those of the pristine material. The rate capability has also been improved at 2 C and 5 C. As a fast lithium-ion conductor with good chemical stability, Li_2ZrO_3 material can form a continuous and uniform coating layer on the surface of active particles, which can inhibit the side reaction between the electrolyte and the electrode material, effectively prevent the corrosion of cathode material by HF attack, and reduce electrode polarization at high rates, leading to the improvement of the specific capacity and the structure stability of Li-rich material.

1 Introduction

In recent years, with the gradual expansion of the electric vehicles field, the secondary batteries in energy storage battery industry has developed rapidly. Lithium-ion batteries have been widely applied in electronic products, traffic power supply and large-scale power storage due to the advantages of relatively safe, high capacity, high monomer voltage, long cycle life and no memory effect.

To achieve a higher energy density, Li-rich manganese-based cathode materials [1–3] have attracted widespread attention because of high capacity, high

Address correspondence to E-mail: wangyuhua@stdu.edu.cn

https://doi.org/10.1007/s10854-021-05503-7

voltage platform and low cost. They are usually represented by $xLi_2MnO_3 \cdot (1-x)LiMO_2$ ($0 < x < 1$, M = Ni, Co, Mn, Fe, etc.), and the molecular formula can also be written as $Li[Li_xM_{1-x}]O_2$. However, there are still some knotty problems to be solved in the practical application of Li-rich materials, such as the high first irreversible capacity loss, oxygen release and structural transformation. These issues are related to more side reactions under high operating voltage (> 4.5 V), the corrosion of the electrode material by HF generated from the decomposition of the electrolyte, and the electrode polarization, leading to the structure instability and reduced capacity.

Several studies have proved that surface coating is an effective modification method to improve the electrochemical performance of cathode materials [1, 4, 5]. Surface coating layer can inhibit the side reaction and improve the stability of the electrodes. Metal oxides and metal fluoride, such as Al_2O_3, TiO_2, and AlF_3 [6–9], are often used as coating materials. In recent years, fast ion conductors, such as Li_3PO_4 [10], Li_2TiO_3 [11], Li_3VO_4 [12], and Li_2ZrO_3 [13, 14], have attracted much attention as coating materials due to they are chemically inert materials with good chemical stability. Among them, Li_2ZrO_3 as a surface coating material has been successfully applied in a variety of cathode materials, and achieved remarkable results. However, there are few studies on Li_2ZrO_3 coated Li-rich materials [15–18]. Moreover, the focus of these limited studies is to improve the electrochemical properties of Li-rich materials, but the corresponding modification mechanism is not clear enough, such as how Li_2ZrO_3 coating material affects the surface morphology or electrode polarization.

In this paper, typical Li-rich material $Li[Li_{0.2}Ni_{0.2}Mn_{0.6}]O_2$ has been successfully modified by Li_2ZrO_3 by a sol–gel method. The properties of the materials modified with different ratios of Li_2ZrO_3 have been discussed including the crystal structure information, surface morphology, and electrochemical properties. Based on electrochemical impedance spectroscopy analysis and cyclic voltammetry, the optimization mechanism of Li_2ZrO_3-modified $Li[Li_{0.2}Ni_{0.2}Mn_{0.6}]O_2$ has also been preliminarily speculated.

2 Materials and methods

2.1 Materials synthesis

The preparation process of the materials is displayed in Scheme 1. $CH_3COOLi \cdot 2H_2O$, $Ni(CH_3COO)_2 \cdot 4H_2O$, $Mn(CH_3COO)_2 \cdot 4H_2O$, citric acid ($C_6H_8O_7 \cdot H_2O$) and ammonia ($NH_3 \cdot H_2O$) were used as raw materials for preparing $Li[Li_{0.2}Ni_{0.2}Mn_{0.6}]O_2$ by a sol–gel method. The mixture of lithium acetate (lithium source excess 5%) and citric acid dissolved in deionized water was named as solution A and the mixture of nickel acetate and manganese acetate dissolved in deionized water was named as solution B. After solution B was added dropwise to solution A, the resulting mixture was continuously stirred to be a homogeneous sol solution. $NH_3 \cdot H_2O$ was employed to adjust the pH of the mixture solution to 7 ~ 8. Then, the mixture solution was heated at 80 °C on the magnetic stirrer to form a gel. After the gel was dried at 200 °C overnight in a vacuum oven, it was evenly ground and placed in a muffle furnace for pre-calcination at 400 °C for 4 h with a heating rate of 4 °C min^{-1}. After grinding the obtained precursor material uniformly, it was calcined in a muffle furnace at 900 °C for 10 h with a heating rate of 4 °C min^{-1} to obtain the pristine material $Li[Li_{0.2}Ni_{0.2}Mn_{0.6}]O_2$.

Based on the pristine sample, Li_2ZrO_3-modified samples were prepared by aqueous solution method. $ZrO(NO_3)_2$ and $CH_3COOLi \cdot 2H_2O$ were dissolved in absolute ethanol in a certain proportion, and the excess of lithium source was 5%. The mixed solution was treated with ultrasonic for 30 min, then added with a certain proportion of pristine material $Li[Li_{0.2}Ni_{0.2}Mn_{0.6}]O_2$, and then ultrasonic for another 30 min. The resulting mixed solution was stirred in a water bath at 80 °C with a magnetic stirrer until the solvent was completely evaporated. The dried mixture was taken out and ground evenly, placed in a crucible, and then calcined in a muffle furnace at 650 °C for 5 h with a heating rate of 5 °C min^{-1}. The modified samples were obtained by grinding the powder evenly. The coating amount was adjusted by controlling the ratio of $ZrO(NO_3)_2$ and $Li[Li_{0.2}Ni_{0.2}Mn_{0.6}]O_2$. The samples with different coating amount of 0 wt.%, 0.5 wt.%, 1 wt.%, and 2 wt.%, were named as NM-0, NM-0.5, NM-1.0, and NM-2, respectively.

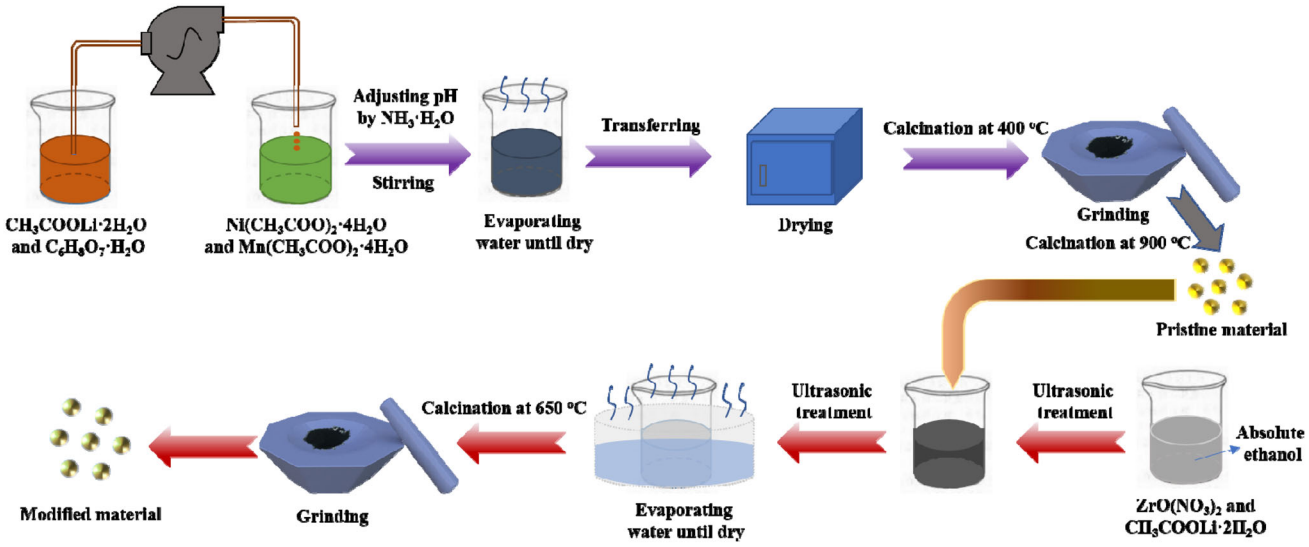

Scheme 1 Preparation process of the pristine material and modified materials

2.2 Materials characterizations

The crystalline structure of the prepared materials was tested using X-ray diffraction (XRD; Bruker, D8ADVANCE) with a Cu Kα radiation source. Data were collected with a step size of 4° min^{-1} in a 2θ range of 10°–90°. The morphology of the prepared powders was observed by a field emission scanning electron microscope (FESEM, Hitachi SU8010). The surface morphology at high magnification of the samples was observed by transmission electron microscope (TEM, JEOL JEM-2100). The chemical states of metal elements were detected by X-ray photoelectron spectrometer (XPS, Thermo Scientific ESCALAB Xi+).

2.3 Electrochemical tests

To prepare the electrodes, the prepared powder, acetylene black, and polyvinylidene fluoride (PVDF) were used as active material, conductor agent, and binder, respectively. The above raw materials were mixed with a weight ratio of 8:1:1 using N-methyl-2-pyrrolidone (NMP) as solvent to obtain uniform slurry. The slurry was coated onto the aluminum foil collector and dried overnight in vacuum at 80 °C. The dried electrode sheet was sliced to obtain a circular electrode sheet with a diameter of 11 mm. The button cells (CR 2025) were assembled in a glove box filled by argon. The prepared circular electrode was used as working electrode, Celgard 2400 was used as separator, and lithium foil was used as counter electrode and reference electrode. The electrolyte employed 1 mol L^{-1} $LiPF_6$ dissolved in organic mixed solvent (EC-DMC, 1:1).

The constant current charge–discharge tests were conducted on the cells in the voltage range of 2 V–4.8 V with different rates (1 C = 20 mA g^{-1}) using Land battery test system (CT2001A, Wuhan, China). Cyclic voltammograms were obtained by electrochemical workstation (CHI660E, Chenhua, Shanghai, China) at a scanning rate of 0.2 mV s^{-1} between 2 V and 4.8 V. Electrochemical impedance spectroscopy was also measured through the electrochemical workstation in a frequency range of 10^5–10^{-2} Hz with an AC perturbation signal of 5 mV.

3 Results and discussion

3.1 XRD structural characterization

XRD patterns of the prepared powders are shown in Fig. 1 to analyze the crystal structure information. All the samples have good crystallinity, and show the characteristic peaks of monoclinic Li_2MnO_3 (C2/m structure) phase in lithium-rich materials in the range of 20–23° [19].The other diffraction peaks belong to the hexagonal layered α-$NaFeO_2$ crystal structure with a space group of $R\bar{3}m$. The position and intensity of diffraction peaks of the modified samples have not changed significantly, indicating that the introduction of surface material had little effect on the crystal structure of bulk material. The high intensity

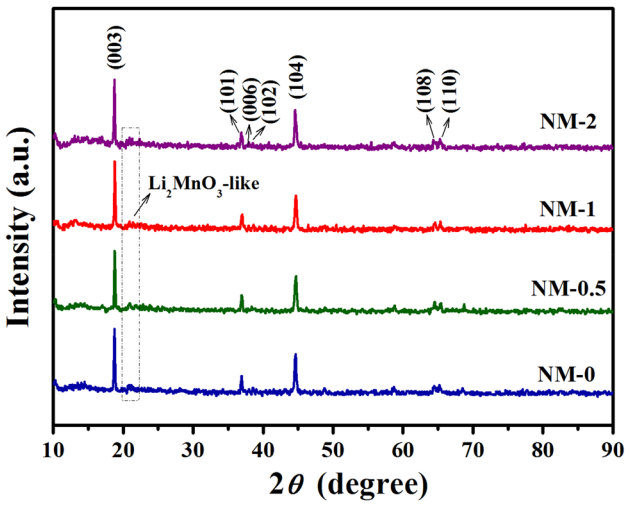

Fig. 1 XRD patterns of the prepared powders with different coating amounts

ratio of (003)/(104) can demonstrate a low cation mixing and good layered structure of Li-rich material [20]. After calculation, NM-1 shows the highest peak intensity ratio of (003)/(104) and its electrochemical performances are expected to be better than the other samples. In addition, no characteristic peaks of Li_2ZrO_3 are found in the XRD patterns of the modified samples, which may be due to the low content of Li_2ZrO_3.

3.2 SEM images

Figure 2 shows SEM images of the prepared samples to compare the morphology. It can be seen that all the prepared samples exhibit typical morphology characteristics of the synthesized materials by sol–gel method. The prepared four powders have irregular spherical particles with the size of 100 ~ 200 nm, and there are some agglomeration and adhesion phenomenon. Some differences can be observed in the surface morphology between the pristine material and the modified material. The surface of the pristine material is very smooth, while the surface of the modified sample becomes rougher with the increase of the coating amount. Some small particles can be observed on the surface of modified particles. Therefore, we preliminarily speculate that Li_2ZrO_3 has been successfully introduced onto the surface of $Li[Li_{0.2}Ni_{0.2}Mn_{0.6}]O_2$.

3.3 TEM images

TEM images in Fig. 3 further shows the surface morphology characteristics of each prepared material. The surface of the pristine material in Fig. 3a is very smooth and there are no small particles covering the surface. However, the surface of the modified materials show different degrees of granular sensation. In Fig. 3b, some small particles surround the surface of NM-0.5 sample, but these particles do not form a uniform coating layer, which may be due to the small amount of coating material. When the coating amount increases, a continuous coating layer is formed on the surface of NM-1 sample, as shown in Fig. 3c. However, when the coating amount is too much, the surface of NM-2 sample in Fig. 3d no longer presents continuous and uniform coating layer, and some small and dispersed particles with high crystallinity appear on the surface. The surface change process of the active particle with different coating amount are illustrated in Fig. 3e. Generally speaking, continuous surface coating layer can better protect the active substances in the electrode materials, reduce the side reaction caused by the contact between the active substances and the electrolyte, and reduce the attack of HF generated by electrolyte decomposition on the active materials, so as to improve the electrochemical performance of the electrode.

The chemical states of Mn, Ni and Zr in NM-0 and NM-1 samples have been measured by XPS. In Fig. 4, it can be seen that the chemical states of Ni and Mn do not change after coating. The Ni $2p_{3/2}$ peak at 854.6 eV with a satellite peak at 860.7 eV is ascribed to Ni^{2+} species.[15] The Mn $2p_{3/2}$ peak at 642.4 eV in the two samples is attributed to Mn^{4+} species.[2, 15] In addition, two strong peaks at 181.9 eV and 184.3 eV observed in Fig. 4f correspond to the typical Zr $3d_{3/2}$ and Zr $3d_{5/2}$ peaks in Li_2ZrO_3, indicating the presence of Zr (+ 4) in the coating layer.[21, 22].

3.4 Electrochemical performances

Figure 5 exhibits the first charge/discharge curves of the four electrodes at 0.5 C. Obviously, all the four electrodes exhibit similar charge–discharge curves. The diagonal platform below 4.5 V corresponds to the extraction of lithium ions from the lithium layer, and this process is also the process in which Ni^{2+} is oxidized to Ni^{4+}. The long plateau at about 4.5 V is a

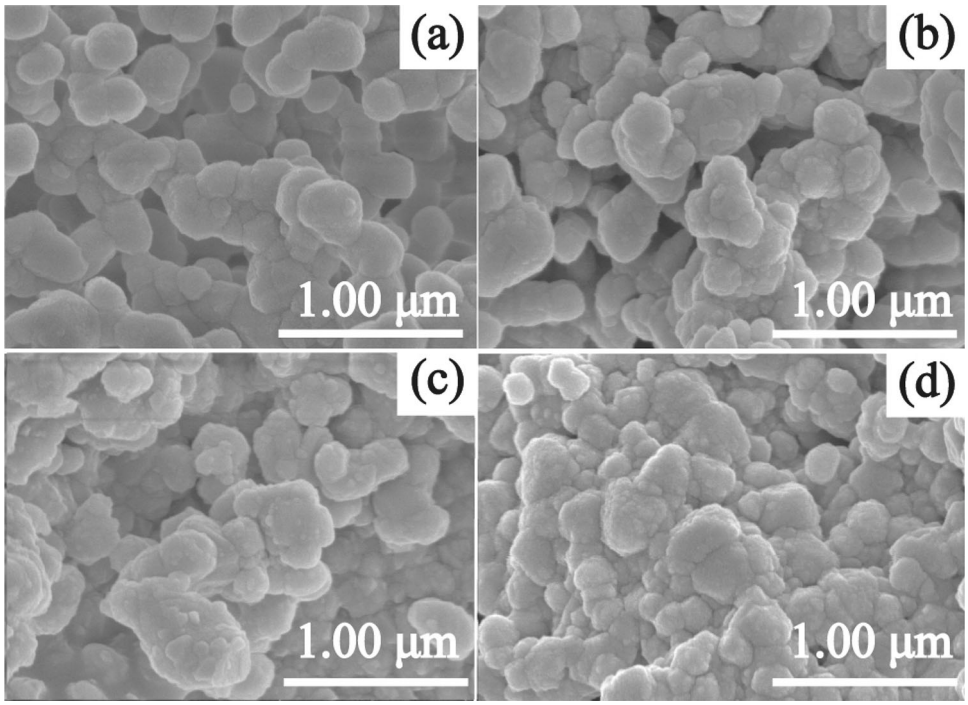

Fig. 2 SEM images of the prepared powders with different coating amounts: **a** NM-0; **b** NM-0.5; **c** NM-1; **d** NM-2

typical feature of the first charge curve of Li-rich materials, which corresponds to the activation of Li_2MnO_3 phase. In this process, lithium ions are extracted from the transition metal layer in the form of Li_2O, accompanied by the irreversible release of oxygen [23]. In Fig. 5, NM-1 shows the highest charge capacity of 272.1 mAh g^{-1} and the highest discharge capacity of 196.1 mAh g^{-1} among the four electrodes. The results indicate that the charge/discharge capacity of Li-rich materials can be effectively enhanced by appropriate Li_2ZrO_3 coating, which may be due to the fact that the surface coating layer can protect the surface of active particles to a certain extent.

Figure 5b, c shows the cycling performances of NM-0 and NM-1 at different rates. After 100 cycles at 0.5 C, NM-1 achieves a high reversible capacity of 182.6 mAh g^{-1} and a high-capacity retention of 94 %. After 200 cycles at 2 C, the reversible capacity of NM-1 is 107.7 mAh g^{-1}, which is also higher than that of NM-0. At 2 C, the capacity retention of NM-1 is 95 %, while the capacity retention of NM-0 is 74 %. Clearly, NM-1 exhibits better cycling stability than NM-0 at 0.5 C and 2 C, benefiting from the protective effect of the coating layer, which can inhibit the corrosion of active particles and maintain the structural stability of the material. Figure 5d compares the rate performance of the electrodes. All the electrodes are first activated at a low rate of 0.1 C for 10 cycles, then cycled at each rate of 0.5 C, 2 C and 5 C for 10 cycles, and finally returned to 0.1 C for 10 cycles. The discharge capacity of the electrode gradually decreases with the increase of discharge rate, which is because the increase of current leads to the increase of internal polarization of the battery. The uncoated sample (NM-0) has high discharge specific capacities of 210 mAh g^{-1} at 0.1 C and 170 mAh g^{-1} at 0.5 C, respectively, which are only lower than those of NM-1 sample. However, the discharge specific capacities of NM-0 sample decrease more severely when cycling at the rates of 2 C and 5 C, which are obviously lower than those of the other modified materials. This may be due to the formation of a thick SEM layer on the surface of NM-0 electrode at a high current, which increases the resistance of the electrode and makes the capacity of the electrode decline faster at a high rate. The rate capability of the modified samples are significantly improved at 2 C and 5 C, especially NM-1 sample. The discharge specific capacities of NM-1 sample are 250 mAh g^{-1} and 75 mAh g^{-1} when the discharge rate are 0.1 C and 5 C, respectively. When the electrode is returned to 0.1 C for cycling, the capacity of NM-1 sample is significantly higher than that of the other samples, and is almost the same as that of the NM-1 sample when activated at 0.1 C. These above results indicate that

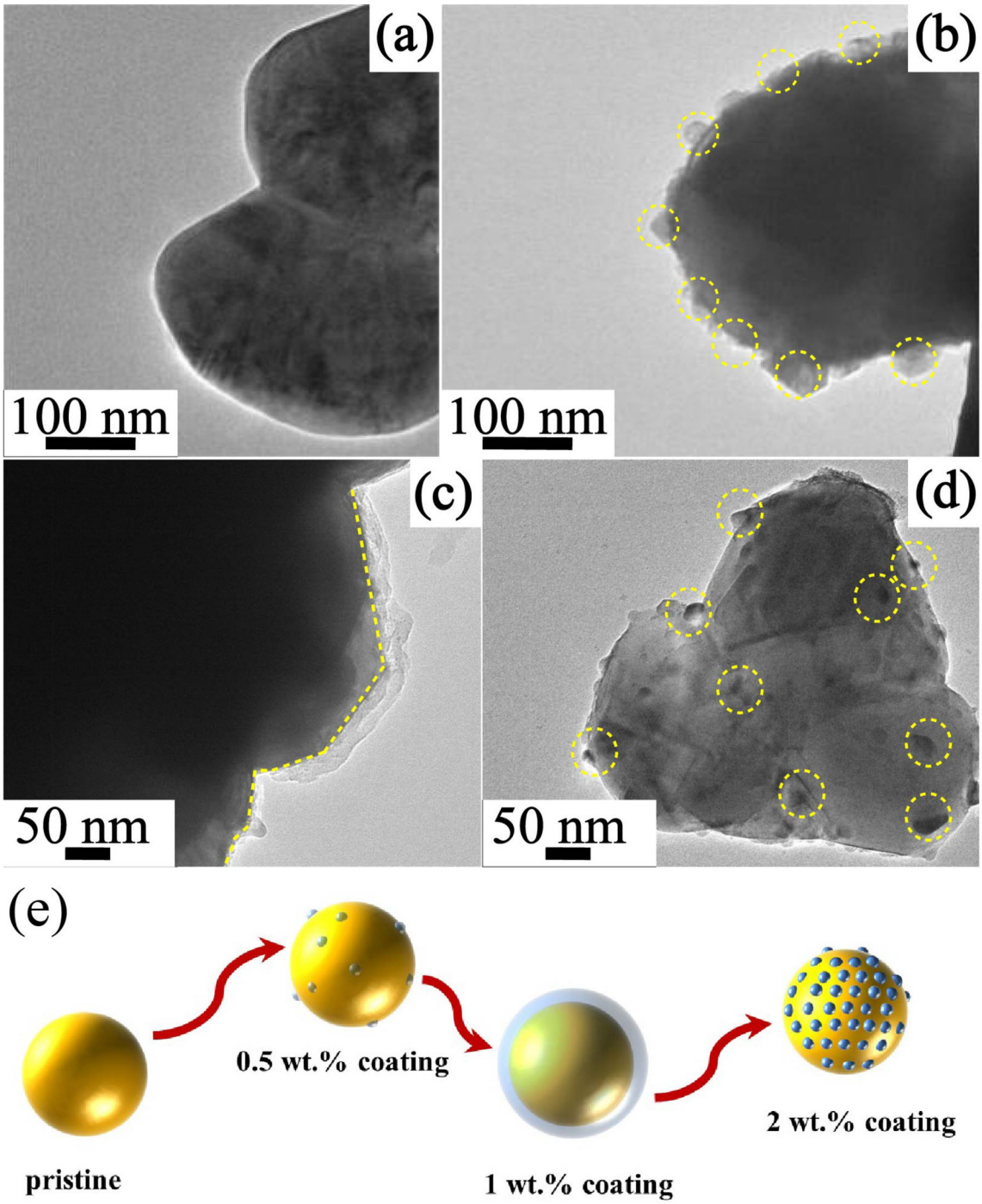

Fig. 3 TEM images of the prepared powders of **a** NM-0, **b** NM-0.5, **c** NM-1, and **d** NM-2, and **e** the corresponding surface change process of active particle

NM-1 sample can withstand repeated charge and discharge process under high current, and can keep stable of the material structure. Therefore, it can be concluded that the appropriate Li_2ZrO_3 coating layer can inhibit the formation of thick SEI film under high current, and increase the structural stability of the Li-rich material, so as to effectively improve the rate capability of electrode material.

Cyclic voltammograms for the first three cycles of the electrodes prepared by NM-0 and NM-1 in Fig. 6a, b reveals the redox behavior in the electrochemical reaction. During the first charging process,

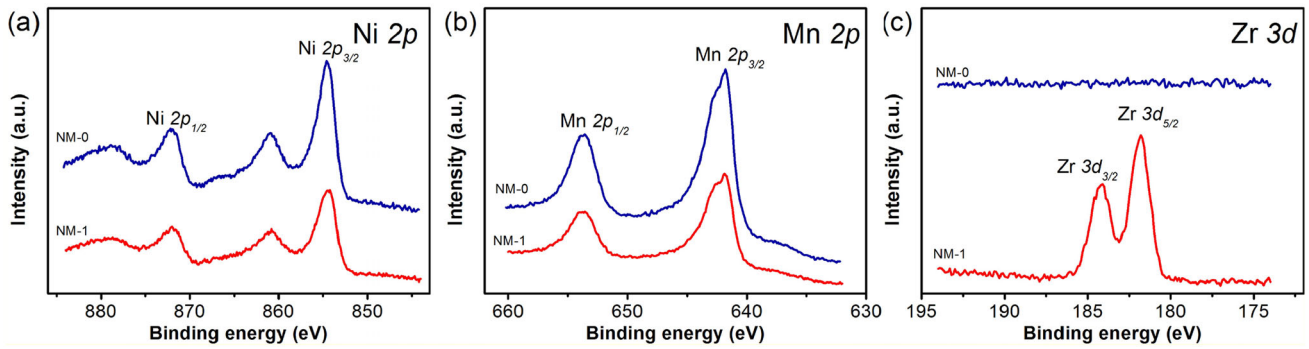

Fig. 4 XPS spectra of Ni 2p, Mn 2p and Zr 3d in NM-0 and NM-1 samples

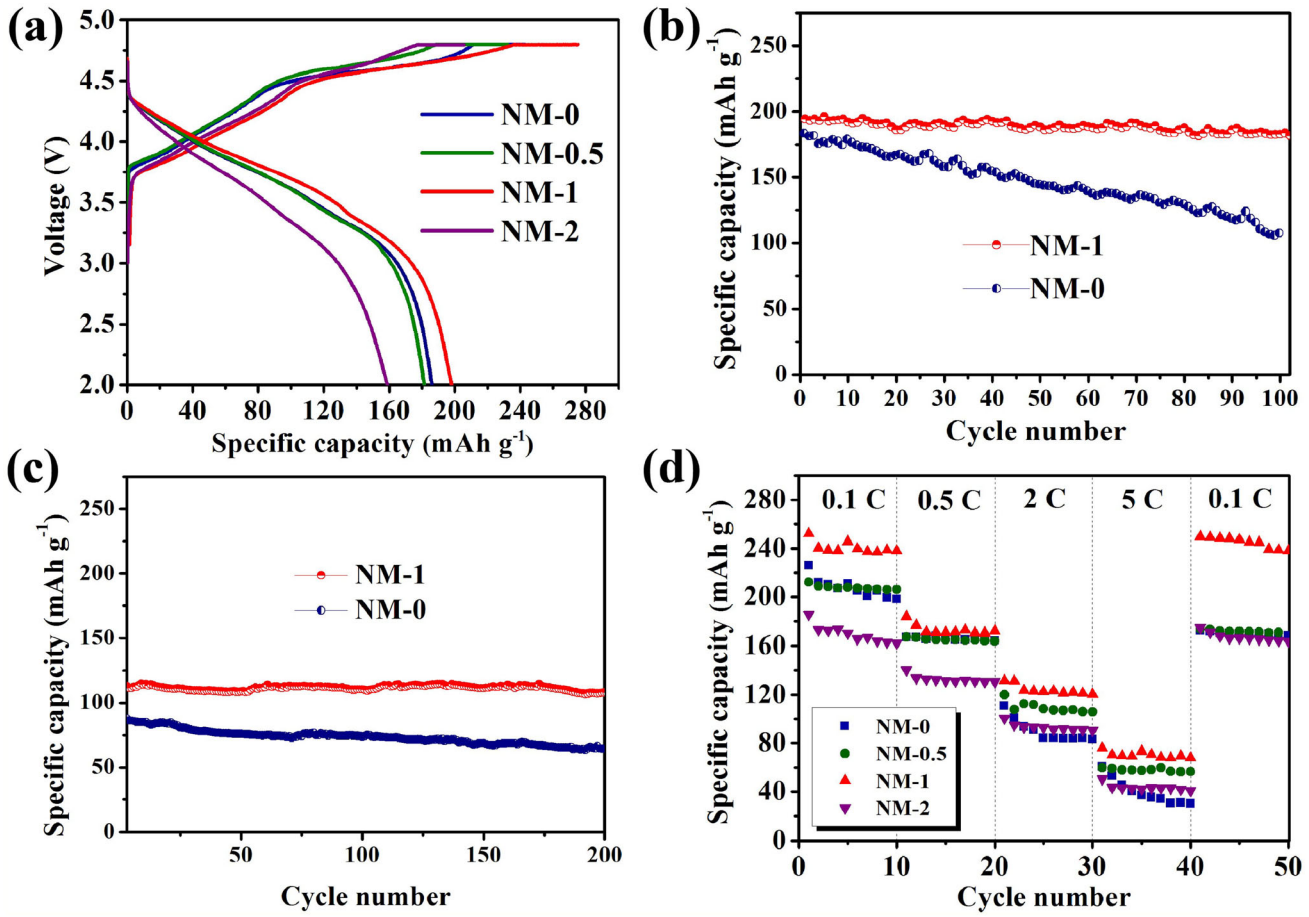

Fig. 5 **a** First charge/discharge curves, **b** cycling performance at 0.5 C, **c** cycling performance at 2 C, and **d** rate capability of the electrodes prepared by different samples

the oxidation peak below 4.25 V corresponds to the oxidation of Ni^{2+} to Ni^{3+} or Ni^{4+}. In addition, the oxidation peak above 4.5 V belongs to the process of lithium extraction and oxygen release in the form of Li_2O, accompanied by the activation of Li_2MnO_3 phase. NM-0 electrode still has a small oxidation peak above 4.5 V in the second and third cycle, indicating that Li_2MnO_3 phase has not been fully activated in the first cycle. As for NM-1 electrode, the 4.5 V peak disappears in the second and third cycles, which indicates that the oxygen release process of the active material in the first cycle is inhibited after Li_2ZrO_3 coating. In the discharge process, the reduction peak around 3.85 V corresponds to the

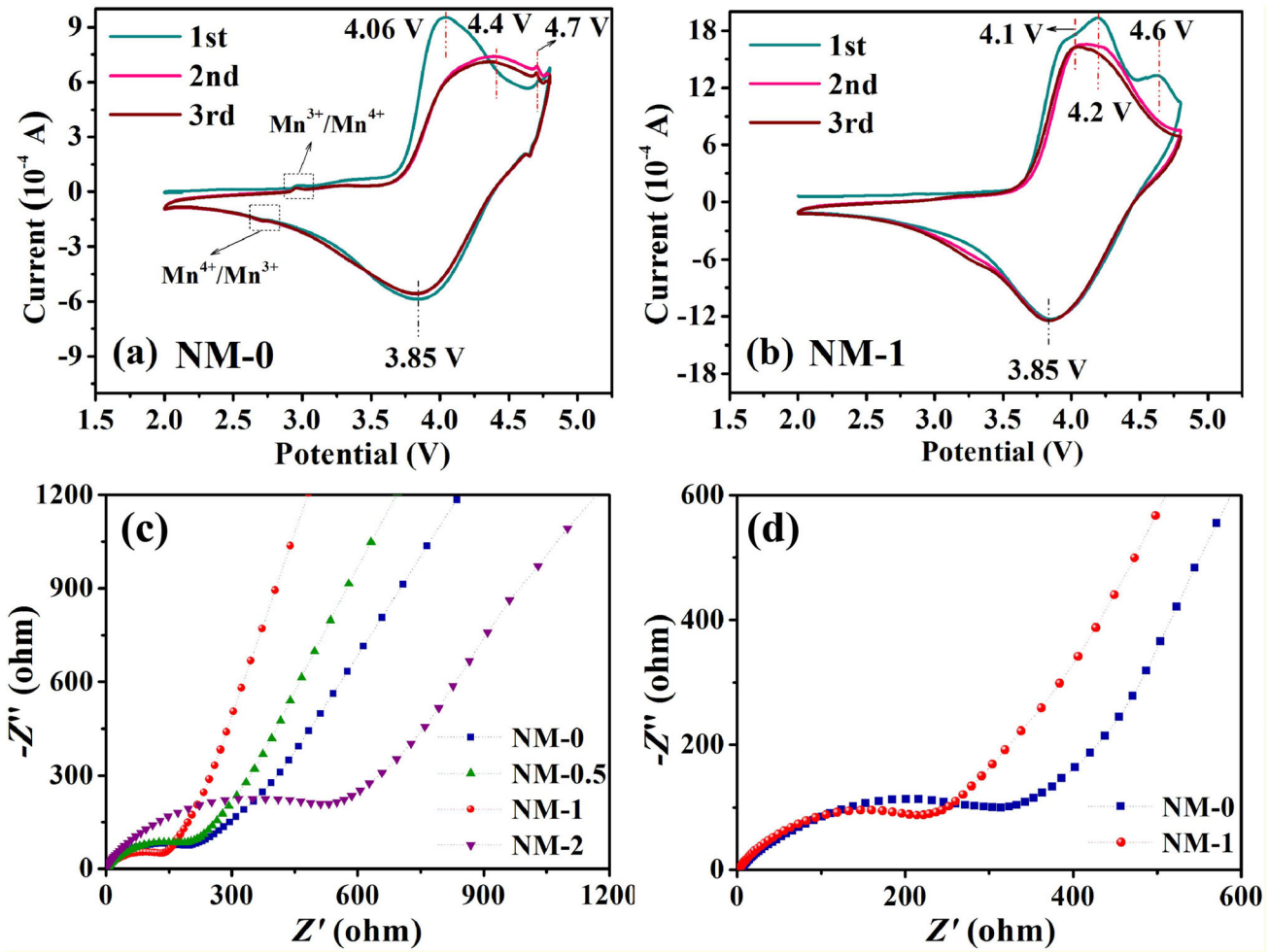

Fig. 6 Cyclic voltammograms for the first three cycles of the electrodes prepared by **a** NM-0 and **b** NM-1 and electrochemical impedance spectra of the electrodes **c** before cycling and **d** after cycling

reduction of Ni^{4+} to Ni^{2+}. From the first discharge process, a pair of reversible redox peaks below 3 V appear in NM-0 electrode, corresponding to the redox reaction between Mn^{4+} and Mn^{3+}, which means the structure transformation from layered to spinel phase (Fig. S1). These redox peaks are not found in NM-1 electrode below 3 V, indicating that Li_2ZrO_3 coating layer can effectively inhibit the structural transformation and maintain the structural stability of Li-rich materials. Moreover, it also can be seen that the potential difference between oxidation peak and reduction peak in NM-1 electrode is obviously smaller than that in NM-0 electrode, revealing that Li_2ZrO_3 coating layer can effectively reduce the electrochemical polarization, thereby improving the electrochemical reversibility of NM-1 electrode.

Figure 6c, d compares EIS of the electrodes before and after cycling. All the EIS curves are comprised of a high-frequency semicircle and a low-frequency slope line, corresponding to the charge transfer resistance (R_{ct}) and diffusion resistance of lithium ions inside the particles, respectively. Generally, the value of R_{ct} reveals the kinetics of electrochemical reaction in the battery. In Fig. 6c, the R_{ct} value of NM-1 electrode before cycling is relatively small, which is 150 Ω. NM-2 electrode shows the highest R_{ct} resistance value, which is about 550 Ω, indicating that excessive coating amount could hinder the electrochemical reaction kinetics. In Fig. 6d, the charge transfer resistance of NM-1 electrode after cycling is obviously lower than that of NM-0 electrode. This may be due to the Li_2ZrO_3 coating layer can effectively improve the structural stability of the Li-rich material and inhibit the side reaction between the electrolyte and the active material.

The electrochemical impedance spectra of NM-0 electrode and NM-1 electrode at different voltages during the first cycle are systematically compared in Fig. 7. First, the fresh battery is charged to 4.8 V at constant current, and then the voltage is maintained at 4.8 V until the current drops to half of the original value. Finally, the battery is discharged to 2 V with constant current. The arrows in Fig. 7a, c indicate the corresponding voltage positions of the tested electrochemical impedance spectra of NM-0 and NM-1 electrode, which are displayed in Fig. 7b, d, respectively. The impedance of the two electrodes changes in a similar way. As in Table S1, the value of charge transfer resistance (R_{ct}) in Fig. 7b, d increases first, then decreases, then increases and finally decreases. The increase of R_{ct} may be related to the formation of SEI film on the electrode surface. The electrochemical impedance at 4.8 V after constant voltage charging (4.8 V-2) is lower than that at 4.8 V before constant voltage charging (4.8 V-1). This is because the electrode polarization reduces in the process of constant voltage charging, which leads to the decrease of internal impedance of the battery. By comparing the two electrodes, it can be found that the R_{ct} values of NM-1 electrode are all significantly lower than that of NM-0 electrode, demonstrating that the Li_2ZrO_3 coating layer can accelerate charge transfer, reduce electrode polarization and improve electrochemical reaction kinetics in the cell, thus improving the electrochemical performance of lithium-rich materials. These results are consistent with the above analysis by CV and charge–discharge data. The improvement mechanism of electrochemical reaction kinetics is speculated as follows. Firstly, as a lithium-ion conductor, Li_2ZrO_3 with high conductivity can accelerate the transfer of lithium ions in the electrode. Secondly,

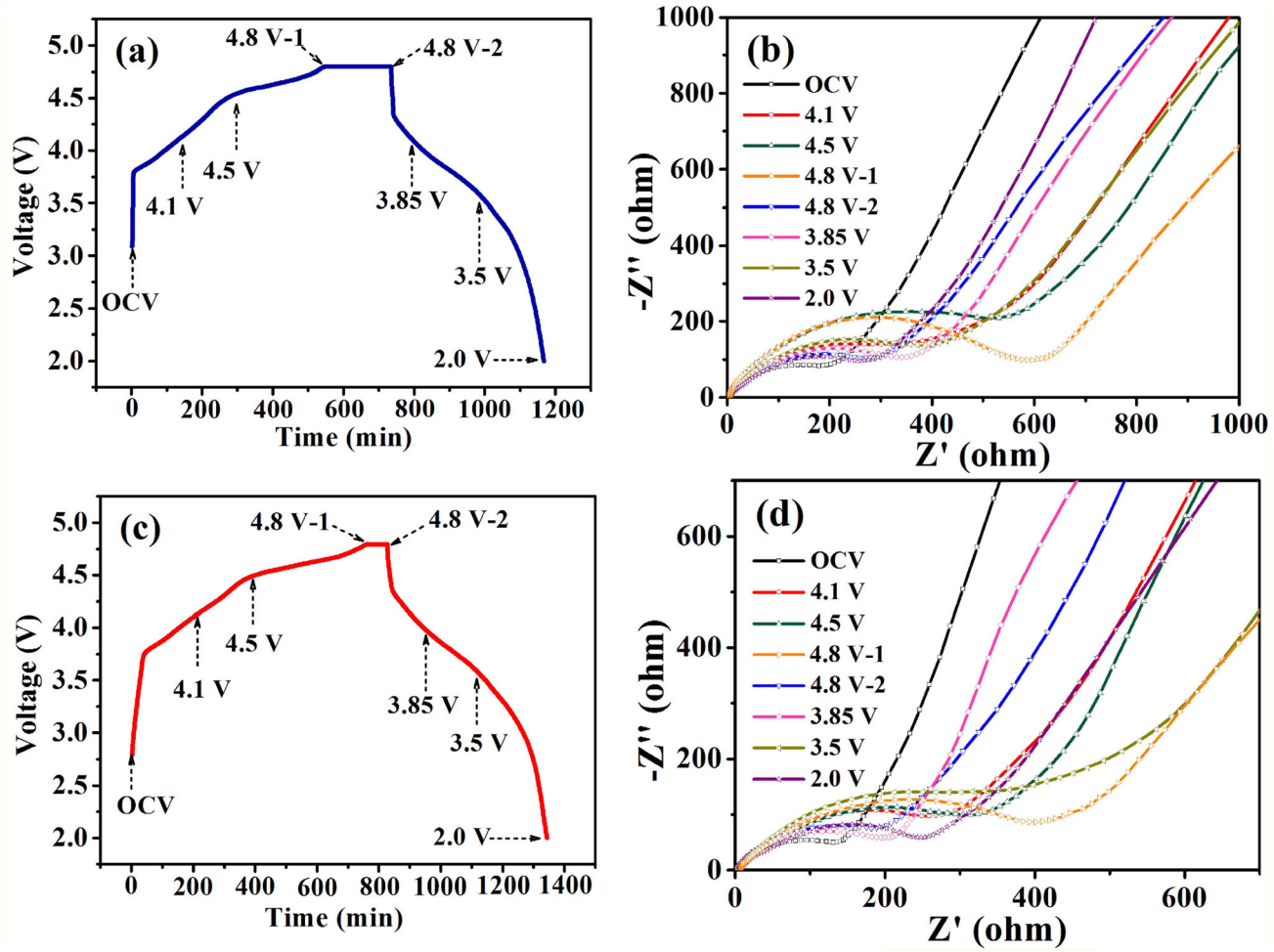

Fig. 7 First charge and discharge curves and the corresponding electrochemical impedance spectra at different voltages of **a**, **b** NM-0 electrode and **c**, **d** NM-1 electrode

the Li_2ZrO_3 coating layer can separate the active material from the electrolyte and reduce the corrosion of the electrolyte to the internal particles.

Figure 8 illustrates the optimization mechanism of Li-rich material modified with surface Li_2ZrO_3 coating layer. The active particle without coating layer withstands more HF attack and side reaction between electrolyte and electrode, leading to the transition metal dissolution issue.[5, 24] Moreover, slow Li^+ diffusion and e^- transport is not beneficial to the charge transfer, resulting in poor high-rate performance. Fast ionic conductor is a kind of material with excellent ionic conductivity, which is realized by ion carriers. Generally, the electronic conductivity of fast ionic conductor is not high.[25] As reported by Hellstrom et al., Li_2ZrO_3 is a relatively good Li-ion conductor with a high conductivity of 3.3×10^{-5} S m^{-1} at 573 K.[26] Moreover, Li_2ZrO_3 possesses three-dimensional tunnels for Li-ion diffusion, excellent intrinsic structural stability and chemical inert. The introduction of surface coating layer causes less HF attack and side reaction on the surface of active particles. Moreover, a thin Li_2ZrO_3 coating layer can suppress the oxygen activity and decrease polarization by introducing strong metal–oxygen bonds which act as the conductive for Li^+.[27] Meantime, Li_2ZrO_3 protective layer can reduce the direct contact between the electrolyte and electrode, thus suppress the dissolution of transition metal elements and side reaction in repetitive lithium insertion and extraction process, which can lead to a higher capacity retention and better cycle life.[28] However, Li_2ZrO_3 is an electrochemical inactive material; so, too much Li_2ZrO_3 on the surface of the material will lead to capacity loss due to a decrease in active material.[29] Therefore, an appropriate coating amount of Li_2ZrO_3 can improve the electrical conductivity of the electrode. That is, appropriate Li_2ZrO_3 coating can accelerate the transmission of electrons and lithium ions in the cathode, thus reducing electrode polarization, and finally effectively improving the electrochemical capacity and rate capability of Li-rich cathode material.

4 Conclusions

The influence mechanism of different Li_2ZrO_3 coating amount on the crystal structure, surface morphology and electrochemical properties of Li-rich material $Li[Li_{0.2}Ni_{0.2}Mn_{0.6}]O_2$ has been systematically studied. The introduction of Li_2ZrO_3 material can maintain the stability of the crystal structure of the active material and change the surface roughness of the active particles. When the addition amount of Li_2ZrO_3 is 1 wt.%, a uniform and continuous coating layer appears on the surface of the modified material. The synthesized material with 1wt.% Li_2ZrO_3 has the best electrochemical performance, including the highest first capacity and rate capability. This may be because the continuous and uniform coating reduces the contact and side reaction between the electrode and the electrolyte and inhibits the corrosion of active materials by HF attack under high voltage, thus achieving the purpose of protecting the active material. In addition, as a fast Li^+ conductor, Li_2ZrO_3 coating layer can effectively reduce the potential difference between oxidation and reduction reaction,

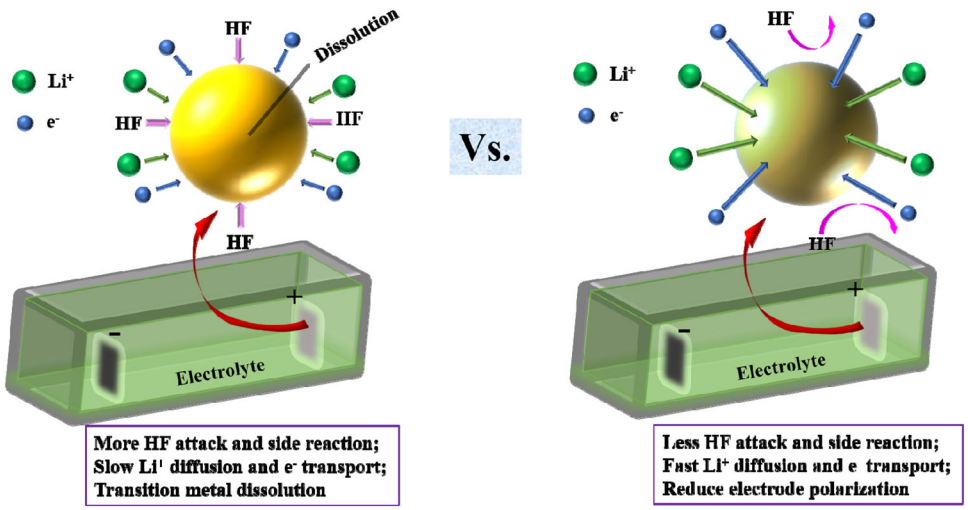

Fig. 8 Optimization mechanism of the Li-rich material modified with surface coating layer

reduce the electrode polarization, accelerate charge transfer, and reduce the charge transfer resistance, thus improving electrochemical performance. Inert materials with good chemical stability have a very broad prospect in modifying electrode materials for rechargeable batteries.

Acknowledgements

This work was supported by the National Natural Science Foundation of China (51902213), Natural Science Foundation of Hebei Education Department (BJ2020046), Natural Science Foundation of Hebei Province (B2016210071), and the Project of Cultivative Innovative Ability of Graduate Students in Shijiazhuang Tiedao University (YC2020061).

Compliance with ethical standards

Conflict of interest The authors have no conflicts of interest to declare.

Supplementary Information: The online version of this article (https://doi.org/10.1007/s10854-021-05503-7) contains supplementary material, which is available to authorized users.

References

1. B. Zhao, J. Xie, H. Zhuang, X. Liu, W. Li, X. Hu, Y. Jiang, J. Zhang, Improved low-temperature performance of surface modified lithium-rich $Li_{1.2}Ni_{0.13}Co_{0.13}Mn_{0.54}O_2$ cathode materials for lithium ion batteries. Solid State Ionics **347**, 115245 (2020)
2. T. Zhao, R. Ji, H. Yang, Y. Zhang, X. Sun, Y. Li, L. Li, R. Chen, Distinctive electrochemical performance of novel Fe-based Li-rich cathode material prepared by molten salt method for lithium-ion batteries. J. Energy Chem. **33**, 37–45 (2019)
3. J.C. Zheng, Z. Yang, P.B. Wang, L.B. Tang, C.S. An, Z.J. He, Multiple linkage modification of lithium-rich layered oxide $Li_{1.2}Mn_{0.54}Ni_{0.13}Co_{0.13}O_2$ for lithium ion battery. ACS Appl. Mater. Interfaces **10**, 31324–31329 (2018)
4. L.M. Zhu, C.G. Bao, L.L. Xie, X.L. Yang, X.Y. Cao, Review of synthesis and structural optimization of $LiNi_{1/3}Co_{1/3}Mn_{1/3}O_2$ cathode materials for lithium-ion batteries applications. J. Alloys Compd. **831**, 154864 (2020)
5. W. Yan, S. Yang, Y. Huang, Y. Yang, Y. Guohui, A review on doping/coating of nickel-rich cathode materials for lithium-ion batteries. J. Alloys Compd. **819**, 153048 (2020)
6. S. Liu, Z. Wang, Y. Huang, Z. Ni, J. Bai, S. Kang, Y. Wang, X. Li, Fluorine doping and Al_2O_3 coating co-modified $Li[Li_{0.20}Ni_{0.133}Co_{0.133}Mn_{0.534}]O_2$ as high performance cathode material for lithium-ion batteries. J. Alloys Compd. **731**, 636–645 (2018)
7. Y. Gan, Y. Wang, J. Han, L. Zhang, W. Sun, Y. Xia, H. Huang, J. Zhang, C. Liang, W. Zhang, Synthesis and electrochemical performance of nano TiO_2(B)-coated $Li[Li_{0.2}Mn_{0.54}Co_{0.13}Ni_{0.13}]O_2$ cathode materials for lithium-ion batteries. New J. Chem. **41**, 12962–12968 (2017)
8. N. Su, Y. Lyu, R. Gu, B. Guo, Al_2O_3 coated $Li_{1.2}Ni_{0.2}Mn_{0.2}Ru_{0.4}O_2$ as cathode material for Li-ion batteries. J. Alloys Compd. **741**, 398–403 (2018)
9. T. Zhao, S. Chen, R. Chen, L. Li, X. Zhang, M. Xie, F. Wu, The positive roles of integrated layered-spinel structures combined with nanocoating in low-cost Li-rich cathode $Li[Li_{0.2}Fe_{0.1}Ni_{0.15}Mn_{0.55}]O_2$ for lithium-ion batteries. ACS Appl. Mater. Interfaces **6**, 21711–21720 (2014)
10. J. Zhu, Y. Li, L. Xue, Y. Chen, T. Lei, S. Deng, G. Cao, Enhanced electrochemical performance of Li_3PO_4 modified $Li[Ni_{0.8}Co_{0.1}Mn_{0.1}]O_2$ cathode material via lithium-reactive coating. J. Alloys Compd. **773**, 112–120 (2019)
11. J. Li, Y. Liu, W. Yao, X. Rao, S. Zhong, L. Qian, Li_2TiO_3 and Li_2ZrO_3 co-modification $LiNi_{0.8}Co_{0.1}Mn_{0.1}O_2$ cathode material with improved high-voltage cycling performance for lithium-ion batteries. Solid State Ionics **349**, 115292 (2020)
12. W. Wang, Z. Yin, Z. Wang, X. Li, H. Guo, D. Wang, Enhanced high voltage electrochemical performance of $LiNi_{1/3}Co_{1/3}Mn_{1/3}O_2$ cathode material by coating with Li_3VO_4. J. Alloys Compd. **646**, 454–460 (2015)
13. J. Zhang, G. Sun, Y. Han, F. Yu, X. Qin, G. Shao, Z. Wang, Boosted electrochemical performance of $LiNi_{0.5}Mn_{1.5}O_4$ via synergistic modification of Li^+-conductive Li_2ZrO_3 coating layer and superficial Zr-doping. Electrochim. Acta **343**, 136105 (2020)
14. B.H. Song, W.D. Li, S.M. Oh, A. Manthiram, Long-life nickel-rich layered oxide cathodes with a uniform Li_2ZrO_3 surface coating for lithium-ion batteries. ACS Appl. Mater. Interfaces **9**, 9718–9725 (2017)
15. K.R. Prakasha, M. Sathish, P. Bera, A.S. Prakash, Mitigating the surface degradation and voltage decay of $Li_{1.2}Ni_{0.13}Mn_{0.54}Co_{0.13}O_2$ cathode material through surface modification using Li_2ZrO_3. ACS Omega **2**, 2308–2316 (2017)
16. X.P. Zhang, S.W. Sun, Q. Wu, N. Wan, D. Pan, Y. Bai, Improved electrochemical and thermal performances of layered $Li[Li_{0.2}Ni_{0.17}Co_{0.07}Mn_{0.56}]O_2$ via Li_2ZrO_3 surface modification. J. Power Sources **282**, 378–384 (2015)

17. Y. Liu, S.L. Shi, G.G.X. Wang, Y. Lu, W.X. Gu, Improved electrochemical properties and thermal stability of $Li_{1.20}Mn_{0.54}Ni_{0.13}Co_{0.13}O_2$ cathode material by Li_2ZrO_3 coating for lithium-ion batteries. J. Mater. Sci. - Mater. Electron. **30**, 18471–18483 (2019)
18. J.C. Zhang, H. Zhang, R. Gao, Z.Y. Li, Z.B. Hu, X.F. Liu, New insights into the modification mechanism of Li-rich $Li_{1.2}Mn_{0.6}Ni_{0.2}O_2$ coated by Li_2ZrO_3. Phys. Chem. Chem. Phys. **18**, 13322–13331 (2016)
19. M. Jiang, B. Key, Y.S. Meng, C.P. Grey, Electrochemical and structural study of the layered, "Li-excess" lithium-ion battery electrode material $Li[Li_{1/9}Ni_{1/3}Mn_{5/9}]O_2$. Chem. Mater. **21**, 2733–2745 (2009)
20. J. Morales, C. Pérez-Vicente, J.L. Tirado, Cation distribution and chemical deintercalation of $Li_{1-x}Ni_{1+x}O_2$. Mater. Res. Bull. **25**, 623–630 (1990)
21. M. Wang, Y.Q. Gong, Y.J. Gu, Y.B. Chen, L. Chen, H. Shi, Effects of fast lithium-ion conductive coating layer on the nickel rich layered oxide cathode material. Ceram. Int. **45**, 3177–3185 (2019)
22. J.F. Ni, H.H. Zhou, J.T. Chen, X.X. Zhang, Improved electrochemical performance of layered $LiNi_{0.4}Co_{0.2}Mn_{0.4}O_2$ via Li_2ZrO_3 coating. Electrochim. Acta **53**, 3075–3083 (2008)
23. A.R. Armstrong, M. Holzapfel, P. Novak, C.S. Johnson, S.H. Kang, M.M. Thackeray, P.G. Bruce, Demonstrating oxygen loss and associated structural reorganization in the lithium battery cathode $Li[Ni_{0.2}Li_{0.2}Mn_{0.6}]O_2$. J. Am. Chem. Soc. **128**, 8694–8698 (2006)
24. S. Zhang, H. Gu, H. Pan, S. Yang, W. Du, X. Li, M. Gao, Y. Liu, M. Zhu, L. Ouyang, D. Jian, F. Pan, A novel strategy to suppress capacity and voltage fading of Li- and Mn-rich layered oxide cathode material for lithium-ion batteries. Adv. Energy Mater. **7**, 1601066 (2016)
25. X.W. Zhan, S. Gao, Y.T. Cheng, Influence of annealing atmosphere on Li_2ZrO_3-coated $LiNi_{0.6}Co_{0.2}Mn_{0.2}O_2$ and its high-voltage cycling performance. Electrochim. Acta **300**, 36–44 (2019)
26. E.E. Hellstrom, W. Van Gool, Li ion conduction in Li_2ZrO_3, Li_4ZrO_4, and $LiScO_2$. Solid State Ionics **2**, 59–64 (1981)
27. H.-K. Song, K.T. Lee, M.G. Kim, L.F. Nazar, J. Cho, Recent progress in nanostructured cathode materials for lithium secondary batteries. Adv. Funct. Mater. **20**, 3818–3834 (2010)
28. W.L. Yao, H.J. Zhang, S.W. Zhong, J.W. Li, L.S. Wang, Facile synthesis of Li_2ZrO_3-modified $LiNi_{0.5}Mn_{0.5}O_2$ cathode material from a mechanical milling route for lithium-ion batteries. J. Electroceram. **43**, 84–91 (2019)
29. M.M. Thackeray, C.S. Johnson, J.S. Kim, K.C. Lauzze, J.T. Vaughey, N. Dietz, D. Abraham, S.A. Hackney, W. Zeltner, M.A. Anderson, ZrO_2- and Li_2ZrO_3-stabilized spinel and layered electrodes for lithium batteries. Electrochem. Commun. **5**, 752–758 (2003)